The Astrophysical Journal, 673:1194–1200, 2008 February 1
© 2008. The American Astronomical Society. All rights reserved. Printed in U.S.A.

SPECTROSCOPIC MEASUREMENTS OF DYNAMIC FIBRILS IN THE Ca II λ8662 LINE

Øystein Langangen, Mats Carlsson,[1] Luc Rouppe van der Voort,[1] and Viggo Hansteen[1]
Institute of Theoretical Astrophysics, University of Oslo, P.O. Box 1029 Blindern, N-0315 Oslo, Norway; oysteol@astro.uio.no

and

Bart De Pontieu
Lockheed Martin Solar and Astrophysics Lab, 3251 Hanover Street, Org. ADBS, Building 252, Palo Alto, CA 94304
Received 2007 June 28; accepted 2007 October 11

ABSTRACT

We present high spatial resolution spectroscopic measurements of dynamic fibrils (DFs) in the Ca II λ8662 line. These data show clear Doppler shifts in the identified DFs, which demonstrates that at least a subset of DFs are actual mass motions in the chromosphere. A statistical analysis of 26 DFs reveals a strong and statistically significant correlation between the maximal velocity and the deceleration. The range of the velocities and the decelerations are substantially lower, about a factor 2, in our spectroscopic observations compared to the earlier results based on proper motion in narrowband images. There are fundamental differences in the different observational methods; when DFs are observed spectroscopically, the measured Doppler shifts are a result of the atmospheric velocity, weighted with the response function to velocity over an extended height. When the proper motion of DFs is observed in narrowband images, the movement of the top of the DF is observed. This point is sharply defined because of the high contrast between the DF and the surroundings. The observational differences between the two methods are examined by several numerical experiments using both numerical simulations and a time series of narrowband Hα images. With basis in the simulations we conclude that the lower maximal velocity is explained by the low formation height of the Ca IR line. We conclude that the present observations support the earlier result that DFs are driven by magnetoacoustic shocks excited by convective flows and *p*-modes.

Subject headings: Sun: atmospheric motions — Sun: chromosphere — techniques: spectroscopic

1. INTRODUCTION

The dynamical nature of the chromosphere is obvious when the Sun is imaged in the line center of strong chromospheric spectral lines, most commonly in the Hα line (e.g., van Noort & Rouppe van der Voort 2006). One of the dominating features is a vast number of thin (0.2–1 Mm) omnipresent jetlike structures (Beckers 1968). On the quiet solar limb they are commonly known as spicules, while on the quiet disk they are often called mottles, and finally in active regions they are known as active region fibrils or dynamic fibrils (DFs). The nomenclature can be confusing, but there are strong indications that these structures are physically closely related (Tsiropoula et al. 1994; Suematsu et al. 1995; Christopoulou et al. 2001; Rouppe van der Voort et al. 2007).

Recently, a combination of high-resolution observations and advanced numerical modeling have shown that DFs are most likely driven by shocks that form when photospheric oscillations leak into the chromosphere along inclined flux tubes (Suematsu 1990; De Pontieu et al. 2004, 2007; Hansteen et al. 2006). The inclination of the magnetic field lowers the acoustic cutoff frequency sufficiently to allow *p*-modes with the dominant low frequencies to propagate along flux tubes (Michalitsanos 1973; Bel & Leroy 1977). These insights into the formation of DFs have become possible because of recent developments in observational techniques, such as bigger telescopes combined with real-time wave front corrections by adaptive optics (AO) systems (e.g., Rimmele 2000; Scharmer et al. 2003b), and postprocessing methods (e.g., von der Luehe 1993; van Noort et al. 2005) which have made observations of these jet structures much more reliable.

These developments have spurred several authors to focus on a detailed understanding of DFs (e.g., De Pontieu et al. 2003, 2004, 2005, 2007; Tziotziou et al. 2004; Hansteen et al. 2006; de Wijn & de Pontieu 2006; Koza et al. 2007; Heggland et al. 2007). One of the important results of this work is that the DFs are driven by and can channel photospheric oscillations into the chromosphere and the corona.

In two papers Hansteen et al. (2006) and De Pontieu et al. (2007) used high-spatial and high-cadence observations of the Hα line center together with realistic simulations to investigate the nature of DFs. One of their conclusions was that the DFs follow parabolic paths along their axis with decelerations lower than the solar gravitational deceleration. Previous observations did not allow an accurate determination of the nature of the trajectory because of lower quality data and line-of-sight (LOS) effects that were difficult to estimate (Nishikawa 1988; Suematsu et al. 1995).

Hansteen et al. (2006) and De Pontieu et al. (2007) further report regional differences between DFs observed in two different plage areas. The regional differences are explained by different inclination angles of the magnetic fields in the two regions. In this way the magnetic topology of the solar atmosphere works as a filter, where only waves with certain periods can leak through. The simulations, spanning from the upper convection zone to the corona, reproduce the observed correlations between the maximum velocities and decelerations in DFs, leading to the conclusion that DFs are formed by chromospheric shocks driven by global *p*-modes and convective flows.

In this paper we add to the understanding of the DFs by analyzing high-spatial and high-cadence spectrograms of the Ca II λ8662 line, put into context by simultaneous Hα spectrograms and narrowband images. Furthermore, the observational results are compared with the numerical simulations of Hansteen et al. (2006).

[1] Also at Center of Mathematics for Applications, University of Oslo, P.O. Box 1053 Blindern, N-0316 Oslo, Norway.

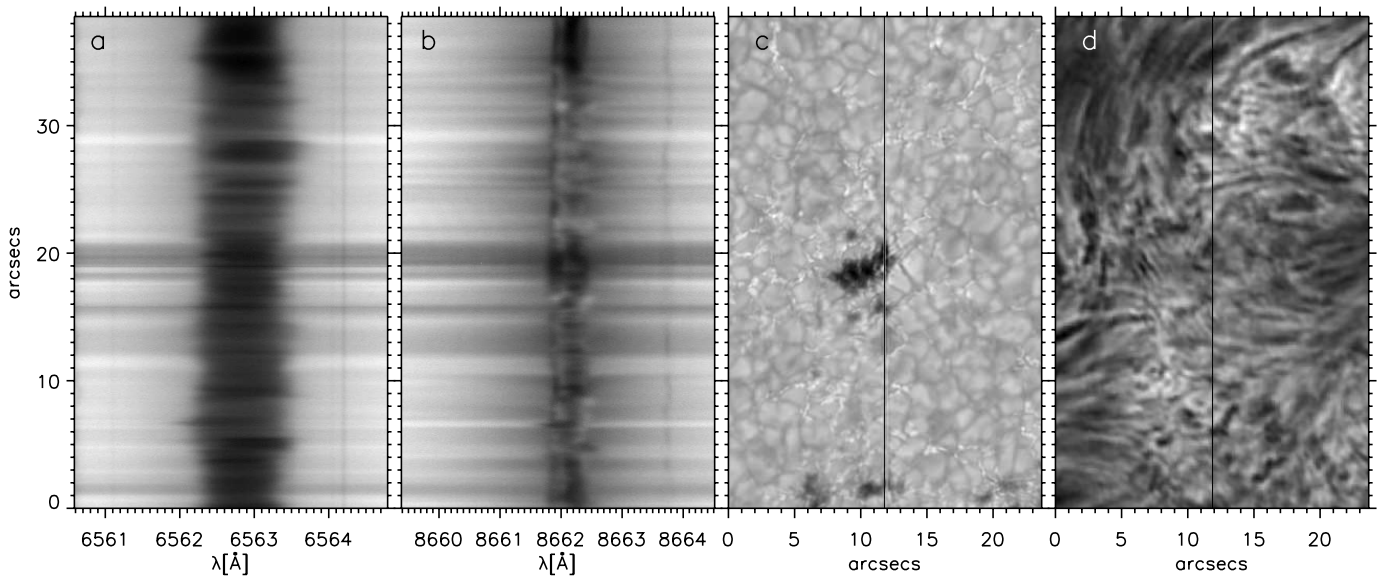

FIG. 1.—Spectrograms of (*a*) the Hα line and (*b*) the Ca II λ8662 line. Notice the highly dynamical line center of the Ca line. (*c*) The corresponding MFBD processed slitjaw image and (*d*) the narrowband Hα DOT image. The position of the spectrograph's slit is marked with a line in the DOT image.

In § 2 we describe the observing program and instrumentation. The data reduction method is described in § 3. In § 4 we show the results of the observations. The main observational errors are discussed in § 5. To get a better understanding of the observations we present several numerical experiments in § 6. Finally, we summarize the results in § 7.

2. OBSERVING PROGRAM AND INSTRUMENTATION

The data presented in this paper were obtained in a coobservation campaign between the Swedish 1 m Solar Telescope (SST; Scharmer et al. 2003a) and the Dutch Open Telescope (DOT; Rutten et al. 2004). The spectrograms were obtained with the SST, using the TRIPPEL spectrograph[2] in combination with the AO system at the SST (Scharmer et al. 2003b). In short, the TRIPPEL spectrograph is a multiport spectrograph, using an echelle grating with a blaze angle of 63.43°. The theoretical spectral resolution is 240000. In our case we observe in two ports to obtain simultaneous Hα and Ca II λ8662 spectra. We observe at −1.06° away from the blaze angle in order 34 and 26, respectively. To remove light from other orders we use two standard filters centered at 6562 and 8680 with FWHM of 43 and 101 Å, respectively. These filters are placed in front of two Megaplus 1.6 cameras (KAF-0401 Image sensor). With this setup the spatial pixel size is 0.041″ pixel^{-1} for both spectral regions, while the spectral pixel size is 0.0105 and 0.0129 Å pixel^{-1} for the Hα and Ca II IR spectral regions, respectively. To obtain a reasonable signal-to-noise ratio we observe with 80 ms exposure times with both cameras. For each of the spectrogram cameras a slit-jaw camera was operated with the same exposure time and with a wideband filter centered close to the corresponding spectrogram wavelength. The filters used were centered at 6565 and 8714 Å and had FWHM of 10 and 100 Å, respectively. These slit-jaw images were used for the destretching of the spectrograms (see § 3). Furthermore, a slit-jaw camera was operated with an exposure time of 8 ms to obtain reference slit-jaw images less blurred by seeing. The filter used was centered at 6565 Å with a FWHM of 10 Å. To get context images for the spectrograms we obtain cotemporal and cospatial observations of both the Hα line center and Hα continuum using the DOT.

On 2006 May 4 we used a small pore in the NOAA active region 10878 (N14°, E04°, $\mu = 0.96$) as AO lock point for the SST (see Fig. 1) to obtain a time series of about 40 minutes (08:20:33–09:01:14 UT) during good to excellent seeing conditions. During this time period we observe in "save all" mode, which in our case means a cadence of ∼0.5 s. All data presented in this paper are from this time series. An overview of the observations can be seen in Figure 1.

3. DATA REDUCTION

3.1. *Aligning, Destretching, and Fourier Filtering*

Flat-field and dark current images were constructed from the mean of 500 images, following the same procedure as described in (Langangen et al. 2007). After these corrections, the spectrograms are aligned to the corresponding wide-band slit-jaw images. This is done by correlating the continuum intensity in the spectrogram and the intensity close to the slit in the slit-jaw image. Furthermore, the continuum images from the DOT are aligned with the slit-jaw images, and since the Hα narrowband images on the DOT are aligned with the continuum images we get a series of aligned spectrograms and both continuum and narrowband images, as seen in Figure 1.

Since the AO is not able to compensate for all the modes in the seeing, especially since the exposure times are 80 ms, postprocessing of the spectrograms as well as the images is desirable. Both the narrowband and wideband DOT images are postprocessed using the speckle method (von der Luehe 1993). The slit-jaw images obtained with 8 ms exposure times are postprocessed using the multiframe blind deconvolution (MFBD; van Noort et al. 2005). Due to the lack of spectral information outside the slit of the spectrograph, a similar reconstruction of the spectrograms is not possible. A partial one-dimensional compensation is, however, possible. The amount of destretching is obtained from the slit-jaw image with the same exposure time as the spectrogram. For this purpose we use the routines developed

[2] See http://dubshen.astro.su.se/wiki/index.php/TRIPPEL_spectrograph.

by Shine et al. (1994). The amount of destretching from the tile covering the slit is then used to destretch the spectrogram. Due to the one-dimensionality of this procedure it is clearly not a complete restoration method, hence the improvements are quite small.

The spectrograms typically have a signal-to-noise ratio of 180 at continuum level. To reduce the noise level we apply a conservative low-pass Fourier filter technique. This reduces the noise significantly (about a factor 2), without losing any significant signal.

3.2. *Wavelength Calibration*

A mean solar spectrogram is constructed by adding the flat-field spectra, altogether 500 exposures. The mean aberration corrected spectrum is then compared to the FTS atlas of Brault & Neckel (1987). This atlas has proved to be well calibrated in wavelength and it shows no systematic offset in line shifts with wavelength (Allende Prieto & Garcia Lopez 1998). Since the solar atlas is corrected for the Earth's rotation, the Earth's orbital motion, and the Sun's rotation, we automatically get a corrected spectrogram when we calibrate using the FTS atlas. Note that in this way our wavelength scale is the same as that of the FTS atlas; we therefore have to correct for the gravitational redshift and the convective blueshift. The convective "blueshift" is in fact a redshift not caused by classical convection in the case of the Ca II IR lines (Uitenbroek 2006). We use the rest wavelength given by the VALD database (Piskunov et al. 1995; Kupka et al. 1999; Ryabchikova et al. 1999). We correct for the gravitational redshift of 634 m s^{-1}. The residual redshift in the mean profile of 425 m s^{-1} is caused by the intensity and velocity variations in the chromosphere, and possibly also by errors in the rest wavelength (Uitenbroek 2006). No correction of this residual redshift is done.

The slit covers a network region of about 38″, or approximately 28 Mm, on the Sun. We have tested the difference between the "quiet" solar atlas and our "active region" mean spectrum. Even though the active region mean spectrum is quite different with respect to the shape of the line profile, the mean line center shift differs only with about 70 m s^{-1}. Since time-dependent variations in the wavelength calibration are known to be quite small we do not use any time dependent wavelength calibration. All in all we estimate the wavelength calibrations to have an accuracy of about 100 m s^{-1}; the errors due to uncertainties in the rest wavelength are, however, of several hundred m s^{-1}.

4. OBSERVATIONAL RESULTS

Since the Hα line is a very wide spectral line with a flat center, it is not very sensitive to Doppler shifts. In addition, the difficulties of understanding the line formation make Hα less than ideal for measuring Doppler shifts and interpreting the results. Instead, we use the Ca II λ8662 line to measure Doppler shifts, only using the Hα line as a reference when we identify DFs. The reader should note that the Ca II λ8662 line also has several disadvantages. First, it has a Fe blend in the blue wing, at 8661.9 Å, that can interfere with large blueshifts in the line center. Second, the line is very dynamic and shows several absorption and emission components, which complicates Doppler measurements. This line is nevertheless suited to measure the Doppler shifts in the DFs, both because it is quite narrow with steep wings and because DFs are easily identified as dark components moving across the line, as seen in Figure 2.

Since the spectrograms suffer from residual seeing effects, the solar features (e.g., DFs, bright points, etc.) will move somewhat both across and along the spectrograph slit. To reduce the effect

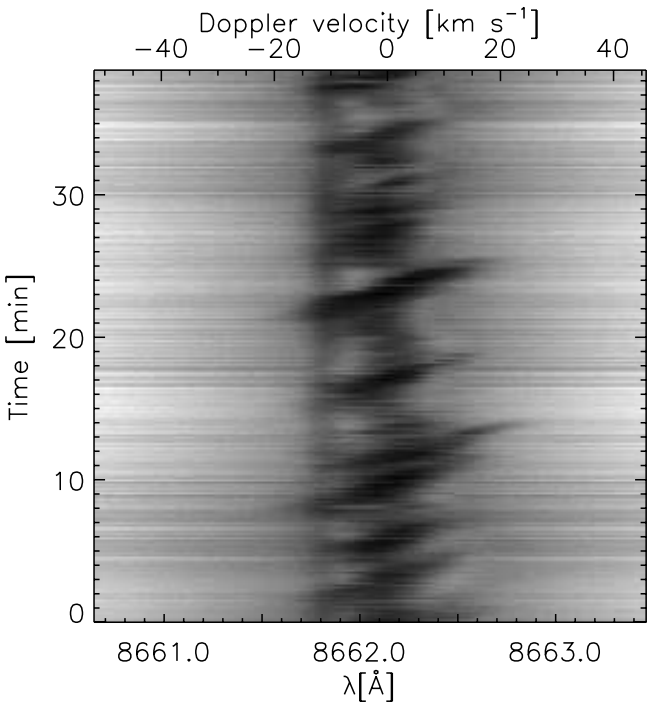

FIG. 2.—Velocity-time plot for the Ca II λ8662 line. Several DFs are seen as diagonal dark components across the spectral line.

of this kind of movement we rebin the spectrograms to a spatial pixel size of 0.12″, and use only the highest contrast images in 6 s bins for this analysis.

To visualize the DFs in a simple way and to make the identification of DFs easier, we make velocity-time (VT) plots (see Fig. 2). The DFs are identified by the diagonal dark components seen in the VT plots. To avoid misidentifications of DFs we only identify DFs above the plage region in the lower part of the continuum images. The narrowband images show that this region clearly contains DFs, but the spatial resolution of the narrowband images is not good enough to measure the motion of independent DFs. Despite the lack of spatial resolution we look for a drop of the intensity in the narrowband images to accept a DF identification. Furthermore, we look for a cospatial and cotemporal component in the Hα spectrograms. In this way we manually identify 26 DFs.

We measure the Doppler shift in these DFs by fitting a fourth order polynomial to the dark component, first appearing in the blue wing, then tracking it through the line center, before it appears in the red wing. The identification of the components is also done manually. The resulting Doppler measurements of the DFs are shown in Figure 3.

A linear polynomial is fitted to each of the observed DFs. Tests with the reduced χ^2 method show that this fit is a good fit if the error is estimated to about 2 km s^{-1}. An error of 2 km s^{-1} is reasonable for these observations.

Accepting the linear fits we can derive a mean value for the deceleration of 89 ± 25 m s^{-2}, for the maximum velocity of 11.3 ± 3.8 km s^{-1}, and lifetimes of 217 ± 39 s, with errors given in one standard deviation. These values are all on the low side of earlier observations, the reason for this discrepancy will be discussed in detail in § 6. It should also be mentioned that the maximum velocity in the receding phase of the DF life seems to have higher values than in the emerging phase, on average 2.4 km s^{-1}

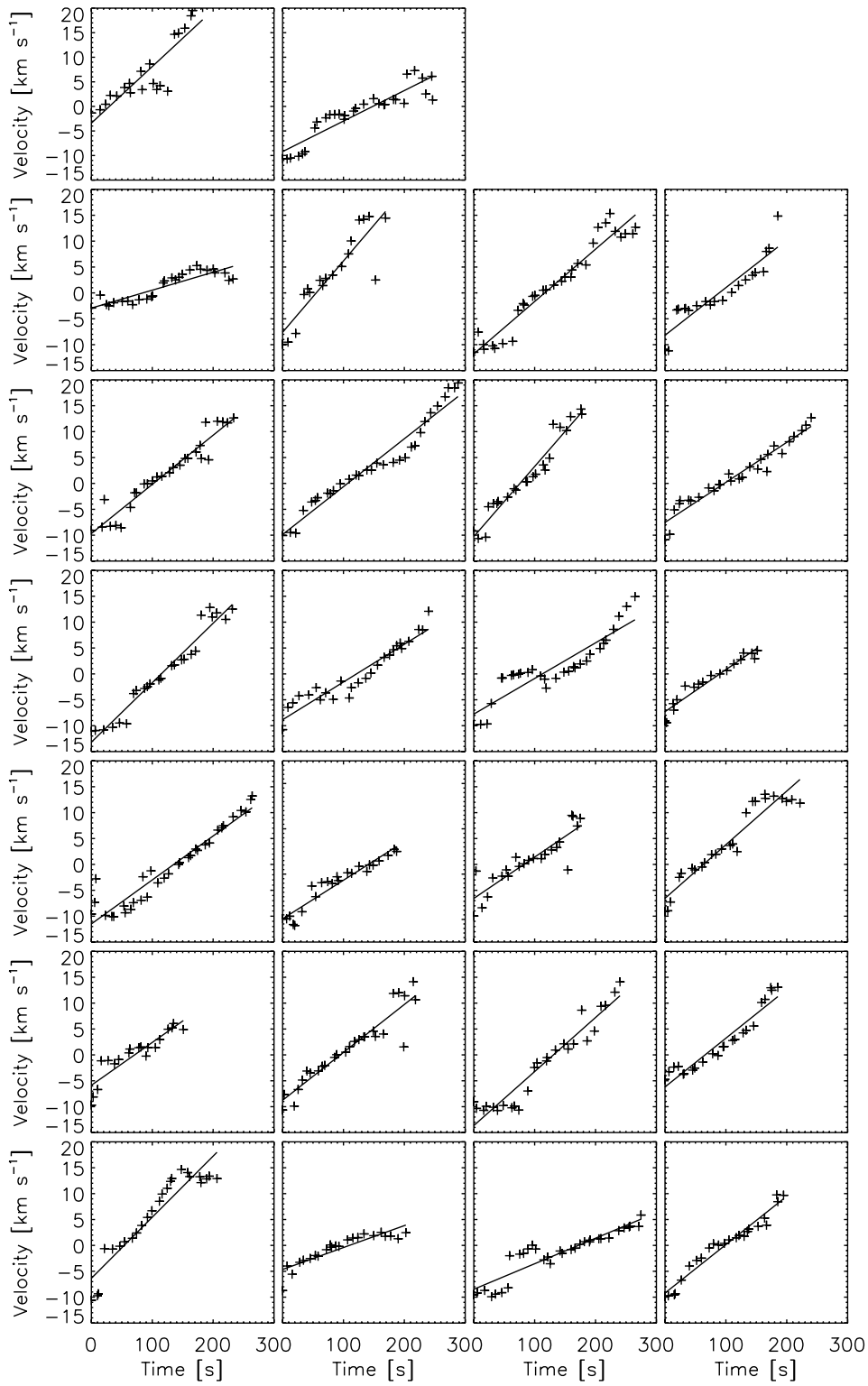

FIG. 3.—Doppler velocities measured in 26 observed DFs (*plus signs*). The least-squares linear fit to these points is plotted as a solid line in each panel.

higher. This result may be caused by the Fe blend in the blue wing of the Ca line.

We get a good correlation between the maximum velocity and the deceleration (see Fig. 4, *bottom*). Using a Spearman rank correlation test (see, e.g., Press et al. 1992) we get a correlation coefficient of 0.82. With the null hypothesis of no correlation we get a significance of 4.1 σ for falsification, which is a fairly strong statistical significance. This correlation has been shown to be a signature of the DF shock theory (Hansteen et al. 2006; De Pontieu et al. 2007; Heggland et al. 2007). The weak negative correlation between the lifetime and the deceleration (see Fig. 4, *top left*) and the weak positive correlation between the maximum velocity and the lifetime, seen in the top right panel of Figure 4, have a statistical weak significance of only 1.4 and 0.9 σ,

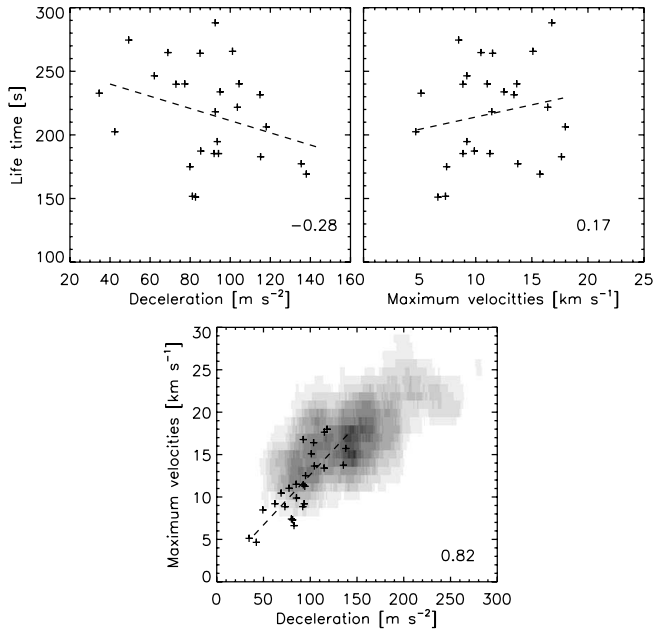

FIG. 4.— Scatter plots of different observables. The linear least-squares fit to the data is plotted as a dashed line. The Spearman correlation coefficients for each scatter plot are shown in the lower right corner of each panel. The data obtained by Hansteen et al. (2006) and De Pontieu et al. (2007) are shown as an inverse gray-scaled density image in the bottom panel.

respectively. Similar weak correlations were found in De Pontieu et al. (2007).

5. ERROR ANALYSIS

The observations presented in this paper differ from previously presented observations of DFs in some fundamental ways. Our data contain the full spectroscopic information, while previous results have usually been based on narrowband images from one or a small number of spectral positions. This makes our observations more robust when it comes to Doppler velocity measurements compared to other methods. Unfortunately this advantage is only achieved at the expense of other disadvantages. In our case there is one main concern, namely the lack of spectral information from regions outside the slit. This lack of information leads to two problems in our analysis. First, parts of the DFs are missed, thus altering the correlations between the observables. Second, it makes us unable to postprocess the observations in a fully consistent way. Nevertheless these observations contain important information about the DF dynamics. Since we cannot correct for these shortcomings we will try to understand their effects on the observations.

To get an estimate of the magnitude and effect on the observables due to the lack of information outside the slit, we investigate an Hα line-core imaging times series, similar to the one presented by De Pontieu et al. (2007). We pick a random "slit" covering a similar plage region as in our spectroscopic observations. We identify 11 DFs crossing the slit, and measure the movement of these DFs. The part of the DFs outside the slit is removed to investigate the effect of the one-dimensional slit. Both the whole DF statistics and the reduced DF statistics show the same correlation between the deceleration and maximum velocity, but the correlation becomes weaker when parts of the DFs are removed. This indicates that the spectroscopic results are still valid, but somewhat affected. The mean values are typically reduced with about 20%. We do expect this effect to be much less severe in Doppler measurements, since we are biased toward DFs that have strong LOS components, and hence are smaller in the image plane compared to the typical DF as seen in a narrowband image. Doppler measurements are usually strongly affected by the point-spread function (PSF), since it contaminates the resolved spectra with other spectra originating from outside the position of the slit. In the present case the PSF is actually making the Doppler measurement more robust. The fact that the high Doppler shifts are seen as a separate component results in a small effect from the PSF on these Doppler measurements. This is because at the wavelength of the separate component other spectra (from neighboring spatial pixels) usually are in the far wing. The low gradient of the far wing results in a small effect on the Doppler component. Since this effect also works vice versa, the high Doppler shifts will show in spectra where it otherwise would not, hence increasing the chances of observing the whole DF.

6. NUMERICAL EXPERIMENTS

To explain the lower velocities and decelerations in the present observations, realistic simulations are needed. The simulation presented by Hansteen et al. (2006) reproduces some of the key results from their observations, and it should therefore be well suited for our purpose. We solve the radiative-transfer equations for the atmospheres given by these simulations. This is done by using the MULTI code (Carlsson 1986). The simulated atmospheres are given in two dimensions, but the problem is simplified by solving for each column independently, each resolving 32.5 km of the solar surface. Each column is solved in full non-LTE for the Ca line, while we include the line blend in LTE, but with a scattering term included in the source function. When solving the radiative transfer complete redistribution is assumed; the results will not be significantly altered by partial redistribution (Uitenbroek 1989).

Since the simulations have several drawbacks, such as instantaneous hydrogen ionization, two-dimensional geometry, and lack of global 5 minute oscillations, it cannot reproduce all details of the DFs. The simulations can nevertheless be used to illustrate the general physics involved. For this purpose we have chosen a DF-like feature in the simulations, which is analyzed in detail. The DF-like feature is identified in a region in the simulations where we have magnetic fields emerging from the photosphere. In this region the flux tubes are fairly vertical, which is similar to the expected inclinations in the observations. Several DF-like features can be identified in this region of the simulations, and most of them show similar behavior to the one we investigate in detail.

Hansteen et al. (2006) and De Pontieu et al. (2007) measure the movement of a bright top, which is caused by the steep temperature increase in the transition region where it is believed that Hα has some contribution. Hence they measure the movement of a point in the image plane that is well defined due to the big contrast seen between the top of the DF and the surroundings. This observational method is compared with the spectroscopic method.

Since the calculation of the response function to velocity (RFV) is based on linear approximations it is not possible to calculate RFV for DFs, which are inherently nonlinear in nature. It is, however, possible to calculate the contribution functions to relative absorption (CFRAs; Magain 1986). The CFRAs are fairly similar to the RFV since the Doppler shifts are seen as an absorption component. We calculate the contribution functions at the Doppler-shifted wavelengths as measured in the different parts of the DF. The resulting contribution functions and the atmospheric velocity, temperature, and density can be seen in Figure 5.

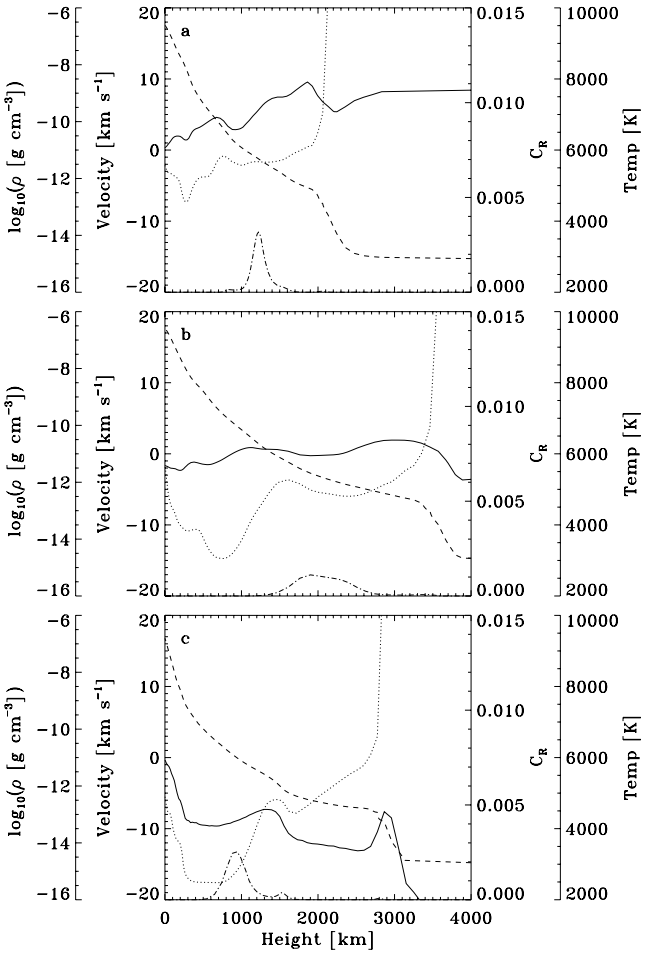

FIG. 5.—Atmospheric parameters for three different times in the life of a DF, (*a*) 20 s , (*b*) 100 s , and (*c*) 160 s . Velocity (*solid line*), temperature (*dotted line*), logarithm of the density (*dashed line*), and finally the contribution functions to relative intensity (*dash-dotted line*) at the Doppler-shifted wavelength are plotted.

The wave seen in Figure 5*a* steepens as the atmospheric density drops about 4 mag from the photosphere into the chromosphere. In the first stage of this DF's lifetime the transition region is found at about 2 Mm. The Ca IR line samples a region below the maximal velocity, which is seen close to the transition region. At this time in the DF the measured Doppler shift is about 6 km s^{-1}, while the velocity close to the transition region is about 10 km s^{-1}. This difference in velocities is very similar to the differences between the observations based on the motion of the transition region and those based on the Doppler shifts (see Fig. 4).

In Figure 5*b* the atmospheric parameters at a later time in this DF's lifetime are plotted. The transition region has been pushed upward by the shock, and it is now at a height of about 3.6 Mm. Even though the formation height of the Ca IR line is somewhat higher in the atmosphere at this stage of the DF lifetime, it is still formed below the transition region. The formation height of the Ca IR line is basically governed by the integrated density above the formation height, hence the reason for the higher formation height at this stage of the DF's lifetime is the higher densities at equal geometric heights. The extension in height of the CFRA is of some significance to the measured Doppler shift, which in this case is close to zero.

In Figure 5*c* the atmospheric parameters at the end of the DF's lifetime is plotted. The transition region height has declined, and is now seen at about 2.8 Mm. The atmospheric velocity close to the transition region is about −13 km s^{-1}, while the measured Doppler velocity is about −8 km s^{-1}. It should be noted that due to the lower height of formation in the Ca IR line the shocks sometimes overlap more than what is seen in the transition region. This leads to sometimes shorter lifetimes in the DFs seen in the Dopplergrams compared to the transition region. Furthermore, some of the movement of the transition region is apparent motion due to sideways motion of the DFs across the slit.

From the analysis above the intrinsic differences in the observational methods can explain the observed differences in maximal velocities. The difference in deceleration can be explained in the shock framework; since the maximal velocities are lower, the deceleration must also be lower assuming similar lifetimes (as mentioned above the lifetimes are somewhat shorter in the spectra, but the relative reduction in lifetimes is smaller then the relative reduction in maximal velocities).

The DFs in the simulated spectra have lower maximal Doppler velocities than in the observations. Typical maximal values in the simulations are 9 versus 11 km s^{-1} in the observations. Furthermore the spread in the maximal velocities in the simulations are lower than in the observations. These differences are in part caused by a central reversal, which makes it impossible to measure the extreme Doppler shifts. The results are lower maximal velocities and lifetimes, but no change in decelerations. These central reversals are caused by the simplified two-dimensional geometry, which neglects the horizontal energy dissipation, hence increasing the temperature in the DFs. Tests from a three-dimensional simulation show that this can account for some of the deficit in velocity, but not all. Other reasons can be differences in inclination angle of the local magnetic field in the observations and simulations. The shorter lifetimes in the simulated DFs, due to lack of global 5 minute oscillations in the simulations will also affect the maximal velocities.

7. CONCLUSIONS

In this work we have presented cospatial and cotemporal narrowband Hα images and spectroscopic measurements of the Ca II λ8662 line. These observations have been used to identify 26 DFs and measure their Doppler shifts. A reduced–χ^2 analysis shows that the time evolution of the Doppler shifts are well approximated by a linear fit, if the measurement errors are about 2 km s^{-1}. Using this approximation we derive values for the decelerations and maximal velocities for each DF. Scatter plots of the deceleration and maximal velocity show a strong positive correlation between the two. We also observe weak correlations between the deceleration and lifetime and the maximal velocity and lifetime. These results support the shock-wave theory as explanation model for the DFs (Hansteen et al. 2006; De Pontieu et al. 2007; Heggland et al. 2007).

Furthermore, the Doppler shifts show that at least a subset of DFs are caused by mass moving up and down in the atmosphere. The values of the maximum velocity and decelerations are all somewhat lower than earlier reported values. Using numerical experiments we have explained the differences in the two observational sets with the intrinsic differences in observational methods. Earlier observations have used the high contrast seen between the top of the DF and the background for measuring the proper motion of the DF. This high contrast is caused by the intensity increase due to contributions from the transition region. In the present observations the DF motion is measured using Doppler shifts, which are affected by the atmospheric conditions over the formation height. The formation height of the Ca II λ8662 line is much lower than the transition region. Since the shock amplitude is increasing from the formation height for the Ca IR line to the transition region, we necessarily measure lower velocities using

spectroscopy. The difference in maximal velocities derived from the two methods in our simulations is about a factor 2, which is about the same as observed. The one-dimensional nature of the slit spectrograph somewhat affects our results, but experiments with narrowband images show that this does not alter the results significantly.

We thank Peter Sütterlin for helping with the acquisition and reduction of the DOT data and Marte Skogvoll for general help with the observations. Ø. L. thanks Margrethe Wold for discussions about the statistical method. This research was supported by the European Community's Human Potential Program through the TOSTISP (contract HPRN-CT-2002-00310) program and by the Research Council of Norway through grant 170935/v30 and through grants of computing time from the Programme for Supercomputing. The Swedish 1 m Solar Telescope is operated on the island of La Palma by the Institute for Solar Physics of the Royal Swedish Academy of Sciences in the Spanish Observatorio del Roque de los Muchachos of the Instituto de Astrofísica de Canarias. The Dutch Open Telescope is operated by Utrecht University at the Spanish Observatorio del Roque de los Muchachos of the Instituto de Astrofísica de Canarias. This research has made use of NASA's Astrophysics Data System.

REFERENCES

Allende Prieto, C., & Garcia Lopez, R. J. 1998, A&AS, 129, 41
Beckers, J. M. 1968, Sol. Phys., 3, 367
Bel, N., & Leroy, B. 1977, A&A, 55, 239
Brault, J., & Neckle, H. 1987, Spectral Atlas of the Solar Absolute Disk-averaged and Disk-Center Intensity from 3290 to 12510 Å (Hamburg: Hamb. Sternw.), ftp://ftp.hs.uni-hamburg.de/pub/outgoing/FTS-Atlas
Carlsson, M. 1986, Uppsala Astron. Obs. Rep., 33
Christopoulou, E. B., Georgakilas, A. A., & Koutchmy, S. 2001, Sol. Phys., 199, 61
De Pontieu, B., Erdélyi, R., & De Moortel, I. 2005, ApJ, 624, L61
De Pontieu, B., Erdélyi, R., & de Wijn, A. G. 2003, ApJ, 595, L63
De Pontieu, B., Erdélyi, R., & James, S. P. 2004, Nature, 430, 536
De Pontieu, B., Hansteen, V. H., Rouppe van der Voort, L., van Noort, M., & Carlsson, M. 2007, ApJ, 655, 624
de Wijn, A. G., & de Pontieu, B. 2006, A&A, 460, 309
Hansteen, V., De Pontieu, B., Rouppe van der Voort, L., van Noort, M., & Carlsson, M. 2006, ApJ, 647, L73
Heggland, L., De Pontieu, B., & Hansteen, V. H. 2007, ApJ, 666, 1277
Koza, J., Sütterlin, P., Kučera, A., & Rybák, J. 2007, in ASP Conf. Ser. 368, The Physics of Chromospheric Plasmas, ed. P. Heinzel, I. Dorotovic, & R. Rutten (San Francisco: ASP), 115
Kupka, F., Piskunov, N., Ryabchikova, T. A., Stempels, H. C., & Weiss, W. W. 1999, A&AS, 138, 119
Langangen, Ø., Carlsson, M., & Rouppe van der Voort, L. 2007, ApJ, 655, 615
Magain, P. 1986, A&A, 163, 135
Michalitsanos, A. G. 1973, Sol. Phys., 30, 47
Nishikawa, T. 1988, PASJ, 40, 613
Piskunov, N. E., Kupka, F., Ryabchikova, T. A., Weiss, W. W., & Jeffery, C. S. 1995, A&AS, 112, 525
Press, W. H., Teukolsky, S. A., Vetterling, W. T., & Flannery, B. P. 1992, Numerical Recipes in FORTRAN, The Art of Scientific Computing (2nd ed.; Cambridge: Cambridge Univ. Press)
Rimmele, T. R. 2000, Proc. SPIE, 4007, 218
Rouppe van der Voort, L. H. M., De Pontieu, B., Hansteen, V. H., Carlsson, M., & van Noort, M. 2007, ApJ, 660, L169
Rutten, R., Hammerschlag, R., Bettonvil, F., Sütterlin, P., & de Wijn, A. 2004, A&A, 413, 1183
Ryabchikova, T., Piskunov, N., Stempels, H., Kupka, F., & Weiss, W. 1999, Phys. Scr., 83, 162
Scharmer, G., Bjelksjö, K., Korhonen, T., Lindberg, B., & Petterson, B. 2003a, SPIE, 4853, 341
Scharmer, G. B., Dettori, P. M., Löfdahl, M. G., & Shand, M. 2003b, SPIE, 4853, 370
Shine, R. A., Title, A. M., Tarbell, T. D., Smith, K., Frank, Z. A., & Scharmer, G. 1994, ApJ, 430, 413
Suematsu, Y. 1990, in Progress of Seismology of the Sun and Stars, ed. Y. Osaki & H. Shibahashi (Berlin: Springer), 211
Suematsu, Y., Wang, H., & Zirin, H. 1995, ApJ, 450, 411
Tsiropoula, G., Alissandrakis, C. E., & Schmieder, B. 1994, A&A, 290, 285
Tziotziou, K., Tsiropoula, G., & Mein, P. 2004, A&A, 423, 1133
Uitenbroek, H. 1989, A&A, 213, 360
———. 2006, ApJ, 639, 516
van Noort, M., Rouppe van der Voort, L., & Löfdahl, M. G. 2005, Sol. Phys., 228, 191
van Noort, M. J., & Rouppe van der Voort, L. H. M. 2006, ApJ, 648, L67
von der Luehe, O. 1993, A&A, 268, 374